

DISCOVERY OF THE COOLEST EXTREME SUBDWARF

ADAM J. BURGASSER¹

Massachusetts Institute of Technology, Kavli Institute for Astrophysics and Space Research, Building 37, Room 664B, 77 Massachusetts Avenue, Cambridge, MA 02139; ajb@mit.edu

AND

J. DAVY KIRKPATRICK

Infrared Processing and Analysis Center, M/S 100-22, California Institute of Technology, Pasadena, CA 91125; davy@ipac.caltech.edu

Accepted to ApJ

ABSTRACT

We report the discovery of LEHPM 2-59 as the coolest extreme M subdwarf (esdM) found to date. Optical and near infrared spectroscopy demonstrate that this source is of later spectral type than the esdM7 APMPM 0559-2903, with the presence of strong alkali lines (including Rb I), VO absorption at 7400 Å and H₂O absorption at 1.4 μm. Current optical classification schemes yield a spectral type of esdM8, making LEHPM 2-59 one of only two ultracool esdMs known. The substantial space velocity of this object ($V_{galactic} \approx -180$ km s⁻¹) identifies it as a halo star. Spectral model fits to the optical and near infrared spectral data for this and four other late-type esdMs indicate that LEHPM 2-59 is the coolest esdM currently known, with $T_{eff} = 2800-3000$ K and $-1.5 \lesssim [M/H] \lesssim -2.0$. Comparison of T_{eff} determinations for M dwarfs and esdMs based on spectral model fits from this study and the literature demonstrate a divergence in T_{eff} scales beyond spectral types ~M5/esdM5, as large as 600-800 K by types M8/esdM8. While this divergence is likely an artifact of the underlying classification scheme, it may lead to systematic errors in the derived properties of intermediate metallicity subdwarfs. We comment on the future of ultracool subdwarf classification, and suggest several ideas for addressing shortcomings in current (largely extrapolated) schemes.

Subject headings: stars: chemically peculiar — stars: individual (LEHPM 2-59, APMPM 0559-2903)
— stars: low mass, brown dwarfs — subdwarfs

1. INTRODUCTION

Subdwarfs are metal deficient stars lying below the stellar main sequence in optical color-magnitude diagrams (Kuiper 1939). Low mass subdwarfs typically exhibit halo kinematics ($\langle V \rangle = -202$ km s⁻¹; Gizis 1997), and are presumably relics of the early Galaxy, with ages $\gtrsim 10$ Gyr. With their extremely long lifetimes (far in excess of the age of the Universe), low mass subdwarfs are important tracers of Galactic structure and chemical enrichment history, and are representatives of the first generations of star formation.

The optical and near infrared spectra of the coolest known M-type subdwarfs, like their solar-metallicity dwarf counterparts, are dominated by molecular absorption, including bands of CO, TiO, AlH, CaH, CrH, FeH, MgH and H₂O (Mould & Hyland 1976; Bessell 1982; Liebert & Probst 1987; Gizis 1997; Leggett, Allard, & Hauschildt 1998; Leggett et al. 2000). Collision induced H₂ absorption (Linsky 1969; Saumon et al. 1994; Borysov, Jørgensen, & Zheng 1997) is also a strong absorber around 2 μm (Mould & Hyland 1976; Leggett et al. 2000). Variations in elemental abundances (i.e., metallicity) can modulate these molecular signatures appreciably, affecting both the total molecular opacity (and hence overall luminosity at a given mass) and relative band strengths through differential chemical abundance patterns and modified atmospheric

chemistry. At optical wavelengths, metallicity effects in subdwarf spectra are seen succinctly in the relative band-strengths of metal oxides and metal hydrides; the former are weaker and the latter stronger in lower metallicity dwarfs (Bidelman & Smethells 1976; Mould & Hyland 1976; Cottrell 1978; Bessell 1982). Current optical classification schemes for M subdwarfs are generally tied to the relative strengths of these bands. For example, the most widely used scheme, that defined by Gizis (1997, hereafter G97), divides metal-poor M stars into subdwarf (sdM) and extreme subdwarf (esdM) classes based on the relative strengths of CaH and TiO bands in the 6300-7200 Å spectral region. G97 and Gizis & Reid (1997) have determined mean metallicities of $[Fe/H] = -1.2 \pm 0.3$ and $[Fe/H] = -2.0 \pm 0.5$ for these two classes of metal-poor dwarfs.

Halo stars exhibit large space velocities relative to the Sun; hence, they are efficiently detected in proper motion surveys. Indeed, most low mass subdwarfs now known were originally identified in blue photographic plate proper motion surveys, particularly those by Luyten (e.g., LHS and NLTT catalogs; Luyten 1979a,b; see also Bakos, Sahu & Németh 2002 and Salim & Gould 2003). With the digitization of the red optical *R*- and *I*-band photographic plate UK Schmidt SERC and AAO (Harley & Dawe 1981; Cannon 1984; Morgan et al. 1992), ESO (West & Schuster 1982; West 1984) and Palomar (POSS-I, Abell et al. 1959; POSS-II, Reid et al. 1991) sky surveys, new proper motion surveys have begun to identify even cooler objects, which emit more of their light at wavelengths redward of the visual band. These surveys – includ-

¹ Visiting Astronomer at the Infrared Telescope Facility, which is operated by the University of Hawaii under Cooperative Agreement NCC 5-538 with the National Aeronautics and Space Administration, Office of Space Science, Planetary Astronomy Program.

ing the Automated Plate Measuring machine Proper Motion survey (Scholz et al. 2000, hereafter APMPM), the Calan-ESO proper motion survey (Ruiz et al. 2001), the SUPERBLINK survey (Lépine, Shara, & Rich 2002; Lépine & Shara 2005) and the SuperCOSMOS Sky Survey (Hambly et al. 2001a,b,c, hereafter SSS) – and associated follow-up programs² have pushed subdwarf discoveries to the end of the M spectral class (Scholz et al. 2004a). Metal-poor analogs to even cooler L dwarfs (Kirkpatrick et al. 1999) have been identified in the SUPERBLINK survey (Lépine, Rich, & Shara 2003a, hereafter LRS03) and serendipitously (Burgasser et al. 2003a; Burgasser 2004) in the Two Micron All Sky Survey (Skrutskie et al. 2006, hereafter 2MASS). These low temperature *ultracool subdwarfs*, encompassing objects with spectral types sdM7/esdM7 and later (Burgasser, Kirkpatrick, & Lépine 2005, see also Kirkpatrick, Henry & Irwin 1997) provide new challenges for atmospheric modeling and extend our sampling of the halo population down to and below the hydrogen burning minimum mass (Burgasser et al. 2003a).

While several ultracool subdwarfs are now known to exist, only one ultracool extreme subdwarf has been found, the esdM7 APMPM 0559-2903 (Schweitzer et al. 1999). To seek out even cooler subdwarfs, we have initiated a program to obtain spectra of red proper motion stars selected from the Liverpool Edinburgh High Proper Motion survey (Pokorny, Jones & Hambly 2003; Pokorny et al. 2004, hereafter LEHPM). One of these sources, LEHPM 2-59, appears to be a later-type esdM than APMPM 0559-2903 based on both near infrared and optical data, and we identify it as the latest-type and coolest esdM found to date. In §2 we summarize the selection of this source from the LEHPM survey. In §3 we describe near infrared and optical spectroscopic observations of this and four other late-type esdMs, and describe their overall characteristics. In §4 we analyze line strengths, radial velocities and spectral types for the optical data, and estimate the distance and kinematics of LEHPM 2-59. In §5 we use spectral model fits to the observed optical and near infrared data to derive T_{effs} and metallicities for the latest-type esdMs. We discuss these results in §6, focusing on the temperature scale of esdMs and future revisions to existing classification schemes for ultracool subdwarfs. Results are summarized in §7.

2. SELECTION OF LEHPM 2-59

The LEHPM catalog is a subset of 11289 proper motion stars from the SSS detected in R -band ESO and UK Schmidt plates covering 7000 deg² of the Southern sky ($\delta \lesssim -20^\circ$). This area excludes regions close to the Galactic plane and those fields with epoch differences less than 3 yr (the mean epoch difference is 8.5 yr). Catalog sources were selected to have $0''.18 \text{ yr}^{-1} \leq \mu \leq 20''.0 \text{ yr}^{-1}$, $\mu/\sigma_\mu > 3$ and $9 \leq R \leq 19.5$, and were cross-matched with photographic B_J and I_N plates (via the SSS) and the 2MASS point source catalog. Further details on the construction and completeness of the LEHPM catalog

are given in Pokorny et al. (2004).

We selected ultracool dwarf and subdwarf candidates from the LEHPM catalog based on red optical/near-infrared color and J -band reduced proper motion (RPM; Hertzprung 1905; Luyten 1922), $H_J \equiv J + 5 \log_{10} \mu + 5 = M_J + 5 \log_{10} V_{tan} - 3.73$. RPM provides a measure of an object's absolute brightness and tangential space velocity (V_{tan}) independent of its (generally unknown) distance, and therefore enables the identification of intrinsically faint and/or halo stars. Optical/near infrared RPM diagrams have become increasingly popular in searches for ultracool nearby and halo stars (Salim & Gould 2002), as these low temperature sources emit more of their flux outside of the optical bands. Here, we focus on the J -band RPM since the spectral energy distributions of late-type dwarfs peak at these wavelengths. Figure 1 displays the H_J versus ($R_{ESO} - J$) diagram for the LEHPM catalog. The main cluster of sources running diagonally down the middle of the diagram is composed primarily of main sequence dwarfs. The smaller cluster of sources offset below and to the left is composed of metal-poor (shifting their colors toward the blue), high velocity (increasing H_J) halo subdwarfs. The smallest grouping in the lower left corner of the diagram is primarily composed of low luminosity white dwarfs.

To select for the latest-type sdMs and esdMs, we applied the following selection criteria to the LEHPM catalog:

- Detection in both R_{ESO} and J bands, and
- $(R_{ESO} - J) \geq 1.5$ and $H_J \geq 19.25$ *or*
- $(R_{ESO} - J) \geq 3.5$ and $H_J \geq 24.5 - 1.5(R_{ESO} - J)$.

The color/RPM criteria are illustrated in Figure 1. Imposing $(R_{ESO} - J) \geq 1.5$ eliminates contamination by the (relatively few) cool white dwarfs; the remaining criteria cordon off the late-type extensions of the dwarf and subdwarf tracks. A total of 50 sources were selected in this manner, including LEHPM 2-59. Of these, 14 have been previously observed by other programs, including 7 M8-M9 dwarfs (Gizis 2002; Lodieu et al. 2005), the sdM7 SSSPM J1930-4311 (Scholz et al. 2004a, a.k.a. LEHPM 2-31) and the esdM6 SSSPM J0500-5406 (Lodieu et al. 2005, a.k.a. LEHPM 1-3861). Results for our complete LEHPM sub-sample will be presented in a forthcoming publication.

3. OBSERVATIONS

3.1. Near Infrared Spectroscopy

LEHPM 2-59 and the three late-type esdMs LP 589-7 (Gizis & Reid 1999, esdM5), LSR 0822+1700 (Lépine, Shara, & Rich 2004, esdM6.5) and APMPM 0559-2903 (Schweitzer et al. 1999, esdM7) were each observed with the SpeX spectrograph (Rayner et al. 2003), mounted on the 3m Infrared Telescope Facility, during three runs on 2004 March 10, 2004 September 5–9 and 2005 December 31 (UT). A log of observations is provided in Table 1. Conditions during these runs ranged from poor (cloudy and high humidity) during 2004 March, to clear with light cirrus during the 2004 September and 2005 December runs. Seeing was typically $0''.5$ – $0''.9$ on all nights. Spectral data were obtained using the prism dispersed mode, which provides low resolution 0.7–2.5 μm

² See Reylé et al. (2002); Lépine, Rich, & Shara (2003a); Lépine, Shara, & Rich (2004, 2003); Rojo & Ruiz (2003); Pokorny, Jones & Hambly (2003); Pokorny et al. (2004); Hambly et al. (2004); Reylé & Robin (2004); Scholz et al. (2004a,b); Deacon, Hambly & Cooke (2005); Lodieu et al. (2005); and Subasavage et al. (2005a,b).

spectra in a single order. Using a $0''.5$ slit, we obtained data with spectral resolution $\lambda/\Delta\lambda \approx 150$ and dispersion across the chip of $20\text{--}30 \text{ \AA pixel}^{-1}$. The slit was oriented to the parallactic angle in all observations to reduce differential color refraction, and the telescope was guided by spillover light from the targets in the imaging channel. Multiple exposures of 180 s each were obtained in an ABBA dither pattern along the slit. Nearby A0 V stars were observed immediately after the target observations and at a similar airmass ($\Delta z < 0.1$) for flux calibration and telluric corrections. Internal flat field and Ar arc lamps were also observed with each target for pixel response and wavelength calibration.

All spectral data were reduced using the SpeXtool package, version 3.3 (Cushing, Vacca, & Rayner 2004) using standard settings. First, spectral images were corrected for linearity, pair-wise subtracted, and divided by the corresponding median-combined flat field image. Spectra were then optimally extracted using default settings for aperture and background source regions, and wavelength calibration was determined from arc lamp and sky emission lines. Individual spectral observations for each science target and A0 star were normalized and combined using a robust weighted mean with 8σ outlier rejection. Data for the A0 stars were also corrected for broad-band shape variations before combining. Telluric and instrumental response corrections for the science data were determined using the method outlined in Vacca et al. (2003), with line shape kernels derived from arc lines. Adjustments were made to the telluric spectra to compensate for differing H I line strengths in the observed A0 V spectrum and pseudo-velocity shifts. Final calibration was made by multiplying the observed target spectrum by the telluric correction spectrum, which includes instrumental response correction through the ratio of the observed A0 V spectrum to a scaled, shifted and deconvolved Kurucz³ model spectrum of Vega.

The reduced near infrared spectra of the four esdMs are shown in Figure 2. These spectra exhibit the characteristic signatures of late-type esdMs, including blue near infrared spectral slopes due to strong collision-induced H₂ absorption; shallow H₂O absorption at 1.4 and 1.9 μm ; FeH and CrH absorption at 0.86, 0.99 and 1.2 μm ; weak bands of TiO at 0.84 μm ; and K I and Na I lines at 0.77, 0.82 and 1.17 μm (Mould & Hyland 1976; Leggett et al. 2000). Notably absent are the deep H₂O and 2.3 μm CO bands that characterize solar-metallicity late-type M dwarfs (Baldwin, Frogel & Persson 1973; Jones et al. 1994, cf. Fig. 1 of Burgasser et al. 2004). The weakness of these bands makes near infrared classification of esdMs difficult (Burgasser et al., in prep.; see §6.2); however, the overall similarity of the spectrum of LEHPM 2-59 to those of LSR 0822+1700 and APMPM 0559-2903, coupled with its stronger H₂O absorption and bluer spectral slope, strongly suggests a late esdM spectral type.

3.2. Optical Spectroscopy

We obtained optical spectroscopy for LEHPM 2-59 and the three late-type esdMs LP 589-7, SSSPM 0500-5406 and APMPM 0559-2903 on 2005 December 4 (UT) using the Low Dispersion Survey Spectrograph (LDSS-3) mounted on the Magellan 6.5m Clay Telescope. A log of

observations is given in Table 2. LDSS-3 is an imaging spectrograph, upgraded by M. Gladders from the original LDSS-2 (Allington-Smith et al. 1994) for improved red sensitivity. The instrument is composed of an STA0500A $4\text{K} \times 4\text{K}$ CCD camera that re-images an $8''.3$ diameter field of view at a pixel scale of $0''.189$. A set of slit masks and grisms allow spectral observations at various resolutions across the optical and red optical band. For our observations, we employed the VPH-red grism (660 lines/mm) with a $0''.75$ (4 pixels) wide longslit to obtain 6050–10500 \AA spectra across the entire chip with an average resolution $\lambda/\Delta\lambda \approx 1800$. Dispersion along the chip was 1.2 $\text{\AA}/\text{pixel}$. The OG590 longpass filter was used to eliminate second order light shortward of 6000 \AA . Two long exposures were obtained for each target, followed immediately by a series of NeArHe arc lamp and flat-field quartz lamp exposures. We also observed a nearby G2-G3 V star after each esdM target for telluric absorption correction.

Data were reduced in the IRAF⁴ environment. We focus our analysis on the blue side of LDSS-3 (in two-amplifier readout mode), covering the 6050–8400 \AA region. Raw science images were trimmed and subtracted by a median combined set of bias frames taken during the afternoon. The resulting images were divided by the corresponding normalized, median-combined and bias-subtracted set of flat field frames. Spectra were then extracted using the APALL task with background subtraction but without variance weighting (i.e., not “optimal extraction”). The dispersion solution for each target was determined using the tasks REFSPEC, IDENTIFY and DISPCOR, and arc lamp spectra extracted using the same dispersion trace; solutions were typically accurate to 0.05 pixels, or 0.07 \AA . Flux calibration was determined using the tasks STANDARD and SENSFUNC with observations of the spectral standard Hiltner 600 (Hamuy et al. 1994, a.k.a. HD 289002) obtained on 2005 December 3 (UT) with the same slit and grism combination as the science data. Corrections to telluric O₂ (6850–6900 \AA B-band, 7575–7700 \AA A-band) and H₂O (7150–7300, 8150–8350 \AA) absorption for each esdM/G star pair were determined by linearly interpolating over these features in the G star spectrum, dividing by the uncorrected G star spectrum, and multiplying the result with the esdM spectrum. These corrections were generally adequate, but noticeable residuals are seen around the O₂ A-band in the spectra of SSSPM 0500-5406 and APMPM 0559-2903, for which G star telluric calibrators were observed at a larger differential airmass. These residuals principally affect the blue wing of the K I doublet at 7665/7699 \AA .

Reduced spectra for the four esdMs observed are shown in Figure 3. Each spectrum shows characteristic spectral traits of late-type esdMs, including weak TiO absorption bands at 6400, 6700 and 7150 \AA (and possibly weak TiO absorption at 7800 \AA); strong CaH bands at 6400 and 6900 \AA ; and prominent line absorption from K I (7665/7699 \AA doublet) and Na I (8183/8195 \AA doublet). The K I doublet lines show substantial broadening in the

⁴ IRAF is distributed by the National Optical Astronomy Observatories, which are operated by the Association of Universities for Research in Astronomy, Inc., under cooperative agreement with the National Science Foundation.

³ <http://kurucz.harvard.edu/stars.html>.

spectrum of LEHPM 2-59, reminiscent of the K I broadening observed in solar metallicity L dwarfs. The 6708 Å Li I line is not detected in any of the spectra; this species has almost certainly been depleted by fusion reactions in the cores of all of these objects. There is a dip in the spectra of SSSPM 0500-5406, APMPM 0559-2903 and LEHPM 2-59 at 7400 Å which we attribute to the 1-0 B⁴Π-X⁴Σ⁻ VO band, a feature commonly observed in solar-metallicity M dwarf and early L dwarf spectra but identified here for the first time in esdM spectra. This detection is robust despite poor telluric O₂ correction in the spectra of SSSPM 0500-5406 and APMPM 0559-2903, as this calibration error affects only the 7600–7700 Å window, while a dip in the spectrum is seen clearly at 7400–7500 Å (see also § 5). Using the Kurucz Atomic Line Database⁵ (Kurucz & Bell 1995), we have also identified a forest of Ca I lines between 6100–6170 and 6440–6500 Å, as well as more prominent lines at 6573 and 7326 Å. All of the atomic features identified in these spectra are listed in Table 3; molecular line identifications can be found in Kirkpatrick, Henry, & McCarthy (1991).

Rb I lines at 7800 and 7948 Å are also present in the spectra of APMPM 0559-2903 and LEHPM 2-59, and the 7948 Å line is weakly present in the spectra of LP 589-7 and SSSPM 0500-5406. These lines are particularly interesting, as they have been previously observed only in the low resolution spectra of L dwarfs (Kirkpatrick et al. 1999) and, more recently, of the esdM6.5 LSR 0822-1700 (Lépine, Shara, & Rich 2004) and the L subdwarf LSR 1610-0040 (Lépine, Rich, & Shara 2003b, however, see Cushing & Vacca 2006; Reiners & Basri 2006). On the other hand, Rb I is not detected in low resolution spectra of the latest-type M dwarfs or sdMs (Kirkpatrick et al. 1999; Lépine, Shara, & Rich 2003; Scholz et al. 2004a). This atomic species is largely ionized in the photospheres of M dwarfs ($T_{ion} \sim 2350$ K; Lodders 1999, 2002), although a significant fraction of Rb I gas is probably neutral at higher temperatures in the higher pressure photospheres of subdwarfs. The appearance of both the 7400 Å VO band and the 7800/7948 Å Rb I doublet lines could be considered a defining trait of ultracool esdMs.

Finally, we note that H α emission, a feature arising from magnetic activity that is nearly always present in the spectra of late-type M dwarfs (Gizis et al. 2000; Hawley et al. 2002; West et al. 2004), is not detected in any of these spectra (including LP 589-7; Gizis & Reid 1999), consistent with weak or absent chromospheres.

4. ANALYSIS

4.1. Atomic Line Strengths and Radial Velocities

Equivalent widths (EWs) for the alkali lines and the two most prominent Ca I lines were measured using the IRAF SPLLOT routine. Uncertainties were determined as the scatter of values from multiple measurements, while upper limits for non-detected lines (Rb I in LP 589-7 and SSSPM 0500-5406) were estimated from the mean EWs of local noise features. These values are given in Table 4. Note that EWs given for the K I and Na I doublets are the combined absorption from both lines in each feature. Nearly all of these lines are seen to strengthen from LP

589-7 to LEHPM 2-59, with the possible exception of the 7326 Å Ca I line, a transition that has the highest lower energy state in Table 3 (4.6 eV; Kurucz & Peytremann 1988). The strengthening of atomic lines is observed in the spectra of solar-metallicity M and L dwarfs as one progresses to later spectral types, and is attributed to lower photospheric temperatures and the corresponding increase in column abundances of these neutral species. The evolution of the line strengths in the esdMs observed here also suggests a trend of cooler T_{eff} with later esdM type.

The six alkali lines and two strongest Ca I lines were used to measure radial velocities (V_{rad}) for the observed sources. Line centers were determined by gaussian fits to the line cores, and velocity shifts were determined relative to the vacuum wavelengths listed in the Kurucz database (Table 3). The mean and standard deviations of these shifts are listed in Table 4, and include a systematic uncertainty of 3 km s⁻¹ based on the mean accuracy of the dispersion solutions. Our values for LP 589-7, SSSPM 0500-5406 and APMPM 0559-2903 are in agreement with those of Gizis & Reid (1999); Lodieu et al. (2005); and Schweitzer et al. (1999), respectively. With $V_{rad} = 79 \pm 9$ km s⁻¹, LEHPM 2-59 also appears to have kinematics consistent with a halo subdwarf.

4.2. Spectral Classification

The optical spectra were classified using the scheme of G97 as updated by LRS03. This scheme is based on the relative strengths of the 7100 Å TiO band and the 6400/6900 Å CaH bands, as sampled by the four indices CaH1, CaH2, CaH3 and TiO5 defined in Reid, Hawley, & Gizis (1995); as well as the redness of the pseudo-continuum in the 6500–8200 Å spectral region as sampled by the Color-M index of LRS03. These indices were measured for each of the spectra after shifting them to their rest frame velocities. Figure 4 compares the combined CaH2+CaH3 indices to TiO5 for these sources, in addition to measurements for late-type dwarfs from Hawley, Gizis, & Reid (1996); G97; Gizis & Reid (1997); Reid & Gizis (2005); LRS03; Lépine, Shara, & Rich (2004); and Scholz et al. (2004a). This index-index diagram, based on work by G97, has been used by several groups to segregate M dwarf spectra by metallicity class. We update the divisions originally set forth by G97 for the combined CaH2+CaH3 indices:

$$sdM : (CaH2 + CaH3) < 1.31(TiO5)^3 - 2.37(TiO5)^2 + 2.66(TiO5) - 0.20 \quad (1)$$

$$esdM : (CaH2 + CaH3) < 3.54(TiO5)^3 - 5.94(TiO5)^2 + 5.18(TiO5) - 1.03. \quad (2)$$

We stress that, as in G97, these divisions are somewhat arbitrary as sources spanning Figure 4 represent a broad continuum of metallicities. Figure 4 nevertheless demonstrates that SSSPM 0500-5409, APMPM 0559-2903 and LEHPM 2-59 are all bona-fide esdMs lying at the tail end of the esdM distribution. LP 589-7 appears to be a borderline sd/esd object; however, for the remainder of this paper we will treat it as an esdM.

Numerical subtypes for the four observed sources were determined using the relations

$$SpT_{esdM} = 7.91(CaH2)^2 - 20.63(CaH2) + 10.71 \quad (3)$$

⁵ Obtained through the online database search form created by C. Heise and maintained by P. Smith; see <http://cfa-www.harvard.edu/amdata/ampdata/kurucz23/sekur.html>.

$$\text{SpT}_{\text{esdM}} = -13.47(\text{CaH3}) + 11.50 \quad (4)$$

(i.e., Eqns. 2 and 8 from G97), and

$$\text{SpT}_{\text{esdM}} = 22.0 \ln(\text{Color} - \text{M}) - 4.1 \quad (5)$$

(i.e., Eqn. 14⁶ in LRS03), where $\text{SpT}_{\text{esdM}}(\text{esdM0}) = 0$, $\text{SpT}_{\text{esdM}}(\text{esdM5}) = 5$, etc. Technically, these relations are defined only up to subtype esdM6 (G97), but we follow current practice (Lépine, Shara, & Rich 2003, 2004; Scholz et al. 2004a; Lodieu et al. 2005) in extrapolating these relations to later numerical types (however, see §6.2). Index values, index subtypes and averages of the numerical subtypes (rounded off to the nearest 0.5 subtype) are listed in Table 5.

The derived subtypes for LP 589-7 and APMPM 0559-2903 are consistent with previous determinations. We derive an esdM6.5 classification for SSSPM 0500-5406, 0.5 subtypes later than the classification given by Lodieu et al. (2005) who measured CaH2 and CaH3 indices 0.05 larger than our values. However, this is generally consistent with the typical uncertainties in index measurements and the corresponding uncertainties in derived spectral types (± 0.5 subtype). For LEHPM 2-59 we derive a classification of esdM8, a full subtype later than APMPM 0559-2903, until now the latest esdM known. This result is consistent with the observed spectral trends noted above, particularly the deeper near infrared H₂O bands and stronger optical atomic lines in the spectrum of LEHPM 2-59. We conclude that LEHPM 2-59 is the latest-type esdM found to date.

4.3. Distance and Space Velocity Estimates

There are currently few late-type esdMs with measured parallaxes; only two sources esdM5 and later (the esdM5 LHS 3061 and the esdM6 LHS 1742a; Monet et al. 1992) have known distances. Hence, only a rough distance estimate (d_{est}) for LEHPM 2-59 is possible. For this, we employed the spectral type/absolute magnitude relations of LRS03 (Eqns. 24 and 25), which can be rewritten as

$$M_R = 10.44 + 0.49(\text{SpT}_{\text{esdM}}) \quad (6)$$

$$M_{K_s} = 8.06 + 0.37(\text{SpT}_{\text{esdM}}), \quad (7)$$

where R is from USNO-B1.0 (Monet et al. 2003) and K_s is from 2MASS. Reid & Gizis (2005) derived a similar relation for M_{K_s} versus spectral type for esdMs,

$$M_{K_s} = 8.73 + 0.31(\text{SpT}_{\text{esdM}}). \quad (8)$$

Assuming $\text{SpT}_{\text{esdM}} = 8$, $R = 18.82$ and $K_s = 14.76$ (Table 7), these three relations yield distances of 79, 55 and 51 pc, respectively. Gizis & Reid (1999) have also derived absolute magnitude/color relations for esdMs; in particular,

$$M_I = 5.96 + 4.29(R - I), \quad (9)$$

where R and I are photographic magnitudes. Again, adopting photometry from USNO-B1.0 ($R = 19.92$, $I = 17.24$) yields $d_{\text{est}} = 79$ pc, in agreement with the M_R /spectral type relation in Eqn. 6. We therefore adopt an average $d_{\text{est}} = 66 \pm 15$ pc for this source, but stress that such estimates are highly uncertain given the current paucity of parallaxes for late-type subdwarfs.

⁶ Note that the LRS03 Color-M/spectral type relation uses the natural logarithm of the Color-M index, and not the base-10 logarithm as suggested by their Eqn. 14.

Using this estimated distance, and the measured proper motion and radial velocity of LEHPM 2-59, we computed UVW space velocity components relative to the Local Standard of Rest (LSR). We derive $[U, V, W] \approx [135, -180, -80]$ km s⁻¹, assuming an LSR solar motion of $[U_{\odot}, V_{\odot}, W_{\odot}] = [10, 5, 7]$ km s⁻¹ (Dehnen & Binney 1998). These velocities lie well outside of the velocity dispersion sphere of local disk M dwarfs ($[\sigma_U, \sigma_V, \sigma_W] \approx [40, 28, 19]$ km s⁻¹ centered at $[-13, -23, -7]$ km s⁻¹; Hawley, Gizis & Reid 1996); and the large negative V velocity, ranging over -210 to -145 km s⁻¹ for our distance estimates, is consistent with motion independent of the Galactic disk. Assuming an LSR rest frame velocity of -220 km s⁻¹ (Kerr & Lynden-Bell 1986), the total space velocity of LEHPM 2-59 in the Galactic potential is 135–190 km s⁻¹. This is well below the Galactic escape velocity in the vicinity of the Sun (Carney, Latham, & Laird 1988; Leonard & Tremaine 1990). Interestingly, the orbit of this object is highly elliptical, and passes well inside the Galactic bulge on its closest approach to the Galactic center. This is not atypical for halo stars currently in the vicinity of the Sun (S. Lépine, 2006, private communication).

5. SPECTRAL MODEL FITS

To further gauge the physical properties of these late-type esdMs, we compared our optical and near infrared spectra to subsolar metallicity theoretical spectral models from Hauschildt, Allard & Baron (1999, NextGen) and Allard et al. (2001, AMES Cond). These models are based on the Phoenix code (Hauschildt, Baron & Allard 1997, and references therein), employ self-consistent temperature/pressure profiles, and assume local thermodynamic equilibrium. Both sets of models use the opacity sampling method; a full account of the chemical species and opacities used by these models is provided in Allard et al. (2001) and references therein. Two major changes in the Cond models are the removal of condensed species from the upper atmosphere and the use of updated TiO and H₂O opacities. The NextGen models and their antecedents (Allard 1990; Allard & Hauschildt 1995; Allard et al. 1997) have been used extensively for fitting M subdwarf spectra (Gizis 1997; Schweitzer et al. 1999; Dawson & De Robertis 2000; Leggett et al. 2000; Lépine, Shara, & Rich 2004).

We sampled grids of NextGen and Cond models spanning temperatures of $2600 \leq T_{\text{eff}} \leq 3600$ K in steps of 100 K, metallicities of $-3.0 \leq [\text{M}/\text{H}] \leq 0.0$ dex in steps of 0.5 dex, and surface gravities of $\log g = 5.0$ and 5.5 cm s⁻². Comparisons were made separately to the optical and near infrared data. For the optical fits, both empirical and model spectra were normalized at 8100 Å as in Figure 3, and the observed data were shifted to their rest frame velocities. For the near infrared fits, data and models were scaled to 1.2 μm. Model spectra were also deconvolved to the resolution of the observed data ($\lambda/\Delta\lambda = 1800$ and 150 for the optical and near infrared, respectively) using a Gaussian kernel. For each spectrum/model pairing, the root mean square (RMS) deviation was computed over the spectral ranges 6050–7500 and 7650–8250 Å in the optical (to avoid regions of poor telluric O₂ correction and the 7400 Å VO band; see below); and 0.75–1.31, 1.45–1.75 and 2.0–2.4 μm in the near infrared (to avoid telluric H₂O regions). The nor-

malization of the model spectra in each fit was allowed to vary by a factor ranging from 0.75 to 1.25 (in steps of 0.05) to allow for continuum offsets, and the normalization with the minimum RMS was retained. For each model set and surface gravity, the T_{eff} and $[M/H]$ combination with the overall minimum RMS was deemed to be the best fit for a particular spectrum. These best fit values are listed in Table 6.

Figure 5 and 6 compares the best fit NextGen and Cond, $\log g = 5.0$ models for the spectrum of LEHPM 2-59 in the optical and near infrared, respectively. Overall, these fits are reasonably good, with the broad spectral shape and several individual features matching quite well. For the optical data, the $\log g = 5.0$ NextGen models consistently provided the best fits to the data. This appears to be largely due to better fits to the 6700 Å CaH band which is only slightly overestimated in the NextGen models but greatly underestimated in the Cond models. The 7150 Å TiO band is too strong in both model sets; higher T_{eff} and/or lower $[M/H]$ models weaken this band but show very poor agreement with the rest of the optical spectrum. TiO features have long been identified as a problem, particularly in the NextGen models (Allard, Hauschildt & Schwenke 2000). Atomic lines are also generally too strong in the best fit models. Indeed, there are many metal lines apparent in the Cond models for which no analogs are seen in the empirical data. The Na I, Rb I and prominent Ca I lines are also too deep, although the K I doublet is reproduced quite well, both in depth and breadth, for both sets of models. The apparent mismatch over 7300-7500 Å is due to the 7400 Å VO band, which is not included in the opacity set of either the NextGen or Cond models (Allard et al. 2001). We found slight systematic effects in the derived parameters between different model sets and surface gravities. The best fit Cond models yielded slightly lower T_{eff} s (by $\lesssim 100$ K) and higher $[M/H]$ values (by $\lesssim 0.5$ dex) as compared to the best fit NextGen models; higher gravity model fits typically gave higher T_{eff} s (by $\lesssim 100$ K) and $[M/H]$ values (by $\lesssim 0.5$ dex).

In the near infrared, spectral model fits again provided reasonably good matches to the broad spectral energy distribution, with slight discrepancies in the 0.99 μm FeH band, the 1.15–1.30 μm continuum (also dominated by FeH absorption in late-type subdwarfs; Burgasser et al. 2004, Cushing et al. 2006; Burgasser et al. in prep.) and the 1.4 μm H₂O band. In this wavelength regime, Cond models typically provided the best fits, largely due to better agreement in the 0.8–1.1 μm region. Systematic shifts in the derived parameters between the NextGen and Cond model sets were less pronounced at these wavelengths, but higher surface gravity models consistently gave larger T_{eff} s (by 100–200 K) and slightly lower $[M/H]$ values (by $\lesssim 0.5$ dex). There was also some degeneracy in the best fit values, with hotter, solar metallicity models providing fairly good matches to the data for $\lambda > 1.1\mu\text{m}$. This is not surprising, given that the blue, relatively featureless near infrared spectra of esdMs are not unlike those of hotter M and K dwarf stars.

Derived parameters between the optical and near infrared fits for a given object exhibit clear systematic differences. T_{eff} s derived from the optical data are generally 100-200 K higher than those derived from the near infrared data; metallicities are consistently 0.5–1.0 dex

higher. Examination of the models indicates that lower metallicities are required to match the H - and K -band suppression in the near infrared data, but can result in optical CaH bands that are too deep. Similar effects are observed with lower T_{eff} s. Since we have no way of independently validating fits in either spectral region, we must treat these systematic differences as a source of uncertainty in the model fits, emphasizing that absolute T_{eff} s and $[M/H]$ values derived from spectral model fits should in general be treated with some caution.

Turning to the derived parameters of the objects in our sample, we find that, overall, later esdM types correspond to cooler T_{eff} s, consistent with expectations. The one notable exception is the esdM6.5 LSR 0822-1700, for which we derive a temperature 100 K cooler than the esdM7 APMPM 0559-2903. This slight difference may not be significant; indeed, our T_{eff} determination based on near infrared data is 200 K cooler than that derived by Lépine, Shara, & Rich (2004) from optical data. However, metallicity effects may be at play. LSR 0822-1700 appears to have a consistently lower $[M/H]$ than APMPM 0559-2903 based on both optical (Lépine, Shara, & Rich 2004) and near infrared analysis. In any case, LEHPM 2-59 is the lowest temperature object in the group, with $T_{eff} \approx 2800$ –3000 K. Evolutionary models by Baraffe et al. (1997) predict a mass of $\sim 0.09 M_{\odot}$ for these parameters assuming an age of 10 Gyr, only $\sim 0.01 M_{\odot}$ above the hydrogen burning minimum mass for these metallicities.

6. DISCUSSION

6.1. *The Temperature Scales of M Dwarfs and Extreme Subdwarfs*

The temperatures derived for late-type esdMs in this and other studies (Schweitzer et al. 1999; Leggett et al. 2000; Lépine, Shara, & Rich 2004) are relatively warm compared to solar-metallicity dwarfs with comparable subtypes, which typically have $T_{eff} \sim 2200$ –2800 K (Kirkpatrick et al. 1993; Leggett, Allard, & Hauschildt 1998; Leggett et al. 2000; Golimowski et al. 2004). Figure 7 compares T_{eff} determinations for M dwarfs and esdMs based on spectral model fits to NextGen models and their antecedents. These data are segregated by optical⁷ (Kirkpatrick et al. 1993; Gizis 1997; Schweitzer et al. 1999; Lépine, Shara, & Rich 2004) and near infrared (Kirkpatrick et al. 1993; Leggett et al. 1996, 2000, 2001; Dawson & De Robertis 2000) analyses. There is a significant downturn in the dwarf T_{eff} scale around type M5–M6, dropping from ~ 3000 K to ~ 2200 K by type M8. The esdMs, on the other hand, show a more gradual decrease in T_{eff} with spectral type over the same range. Linear fits to optical and near infrared T_{eff} determinations over the range esdM1–esdM8 yield parallel relations:

$$T_{eff} = 3750 - 93 \times \text{Sp}T_{esdM} \text{ K (optical)} \quad (10)$$

$$T_{eff} = 3620 - 96 \times \text{Sp}T_{esdM} \text{ K (near infrared)} \quad (11)$$

with dispersions of 30 and 90 K, respectively. The temperatures of the two latest esdMs, APMPM 0559-2903

⁷ We did not include T_{eff} determinations for M dwarfs later than M6 in the Kirkpatrick et al. (1993) and G97 studies due to the poor quality fits to ultracool dwarf spectra existing models provided at that time.

and LEHPM 2-59, are 600–800 K hotter than those of equivalently typed solar-metallicity dwarfs.

Why would the effective temperatures of ultracool esdMs differ so greatly from those of ultracool solar metallicity dwarfs? It is well known that lower metallicity implies lower overall atmospheric opacity, a consequence of reduced molecular and H^- abundances. Hence, for a given mass, the observed photosphere lies at deeper, hotter and higher pressure layers in more metal-poor stars. However, this argument serves only to explain (possible) differences in T_{eff} /mass relations between metallicity classes. T_{eff} /spectral type relations also hinge on how the spectral types themselves are derived. In fact, the classification of M dwarfs and esdMs are determined by separate relations in the G97 and LRS03 schemes, as necessitated by the divergence of spectral properties between these metallicity classes. Hence, differences in the T_{eff} /spectral type relations between M dwarfs and esdMs may simply be an artifact of the underlying classification scheme. At first glance, this may seem unimportant, for as long as the correct scale is used for a given metallicity class, one should derive the correct T_{eff} . However, metallicity is not a discrete quantity like metallicity class, and systematic deviations can occur for individual objects that are more or less metal-poor than the mean of their assigned class. A more global T_{eff} /metallicity/spectral type relation is required.

6.2. Future Prospects for Ultracool Subdwarf Classification

With the recent compilation of several red optical proper motion surveys and the initiation of near infrared programs (Deacon, Hambly & Cooke 2005, Looper et al., in prep.), it is quite likely that LEHPM 2-59's status as the coolest esdM known will not be long-lived. Indeed, the identification of a few L subdwarfs (sdL) to date suggests that esdL discoveries may not be far off (however, see below). It has been shown by Burgasser et al. (2003a) and Lépine, Rich, & Shara (2003b) that these ultracool metal-poor stars and brown dwarfs cannot be adequately classified by existing schemes largely due to the disappearance of the 7150 Å TiO band. The lack of flux from these cool objects also argues against classification in the 6300-7200 Å region.

So where do we proceed? An obvious option is to define new subdwarf classification schemes at longer wavelengths, including the red optical (cf. late-M and L dwarfs) and near infrared (cf. T dwarfs) spectral regions. Absorption bands from the metal hydrides FeH and CrH (and perhaps TiH; Burrows et al. 2005) are prominent in ultracool dwarf and subdwarf spectra for $\lambda > 8000$ Å, and are likely to be present in even lower metallicity analogs. Contrasting these features with longer wavelength TiO (8200 and 8400 Å) and VO bands (7900, 9500 and 10500 Å), alkali lines (Na I, K I, Rb I and Cs I) or pseudo-continuum slope should prove to be effective diagnostics for segregating metallicity and temperature classes. At longer wavelengths, subdwarf classification becomes more difficult due to the weakness of absorption features and the strong suppression of *H*- and *K*-band flux by H_2 absorption (which also wipes out the 2.3 μm CO band). Nevertheless, ratios comparing the 1.4 μm H_2O band and the near infrared spectral slope might provide some dis-

crimination (Burgasser et al. in prep.), while metal line features (including Al I; see Cushing & Vacca 2006) and FeH bands in the 1-1.35 μm region could be used for higher resolution studies.

As later extreme subdwarfs are identified, what will define the termination of the esdM class and the beginning of the esdLs? Solar-metallicity L dwarfs are distinguished by waning metal oxide bands, strengthening metal hydride and alkali lines, steep red optical slopes and red near infrared colors. Yet esdMs already exhibit weak metal oxides and strong metal hydrides, and several neutral alkali species (including Rb I and Cs I); while near infrared colors will never become red due to strong absorption by H_2 (Saumon et al. 1994). Spectral models cannot provide clear guidance on this transition, as it remains unclear as to whether condensate formation, a key aspect of the M/L dwarf transition, plays a significant role in low-temperature metal-poor atmospheres (Burgasser et al. 2003a). Clearly, cooler extreme subdwarf discoveries must guide the definition and our understanding of this transition.

One further complication in this issue is whether halo esdLs even exist in our Galaxy today. As metal-poor halo objects about the substellar mass limit evolve over ~ 10 Gyr, wide gaps in the luminosities and effective temperatures of this population develop. Low mass stars attain a steady-state $T_{\text{eff}} \gtrsim 2500$ -3000 K, while most brown dwarfs cool to $T_{\text{eff}} \lesssim 1000$ K in this time (Burrows et al. 2001, cf. Figure 3 in Burgasser et al. 2003a). Only a narrow range of low mass star/brown dwarf transition objects are expected to encompass intermediate L-type T_{eff} s between these limits, and could therefore be quite rare. Future surveys for low luminosity metal-poor objects will hopefully probe this L dwarf gap, providing, if little data for esdLs, a unique constraint for brown dwarf evolutionary theories.

Finally, one area in which subdwarf classification can be immediately improved is the identification of specific standard stars for temperature and metallicity subtypes. A framework of standard stars is a fundamental tenet of the MK Process (Morgan, Keenan & Kellman 1943; Morgan & Keenan 1973; Keenan & McNeil 1976; Corbally, Gray & Garrison 1994), the most widely adopted method of stellar classification. Standard stars provide the basis of current classification schemes for solar metallicity M (Kirkpatrick, Henry, & McCarthy 1991), L (Kirkpatrick et al. 1999) and T dwarfs (Burgasser et al. 2006). Allowing specific stars to define a classification scheme provides a level of consistency that is not generally present in pure index schemes, while retaining independence from constantly evolving theoretical interpretations. There are now several dozen M subdwarfs of types sdM5/esdM5 and earlier from which appropriate standards can be chosen, and we anticipate that current red optical and near infrared proper motion surveys will soon fill in the remainder of the M subdwarf and extreme subdwarf sequences. Now is an opportune time to consider the construction of a more robust classification scheme for late-type subdwarfs.

7. SUMMARY

We have identified LEHPM 2-59 as the coolest esdM identified to date. Near infrared and optical spectroscopy show features indicative of a late-type esdM, including

strong alkali lines, VO and H₂O absorption and a blue near infrared spectral slope. We derive an optical spectral type of esdM8 on the G97 and LRS03 schemes, and spectral model fits to both optical and near infrared data indicate $T_{eff} = 2800\text{--}3000\text{ K}$ and $-1.5 \lesssim [M/H] \lesssim -2.0$ for this source. Its kinematics confirm it as a halo star. We show that the temperatures of this and other late-type esdMs are significantly higher than equivalently classified solar-metallicity M dwarfs, a divergence that could lead to systematic errors in derived parameters for objects with intermediate metallicities. Finally, we have touched on the future prospects of M subdwarf classification, and methods by which it may be improved and extended to later subtypes. With the current high discovery rate of low-temperature, ultracool halo subdwarfs, it is likely that these issues will require further scrutiny in the near term.

We thank P. Hauschildt and F. Allard for making their team's spectral models electronically available, and acknowledge useful discussions with P. Hauschildt, S.

Lépine, S. Mohanty and J. Mulchaey during the preparation of the manuscript. We also thank our anonymous referee and our scientific editor, J. Liebert, for their helpful comments. AJB acknowledges the assistance of telescope operators B. Golisch, D. Griep and P. Sears at IRTF, and H. Rivera and S. Vera at Magellan during the observations presented in this study, as well as our instrument scientists J. Rayner (SpeX) and J. Bravo (LDSS-3). This publication makes use of data from the Two Micron All Sky Survey, which is a joint project of the University of Massachusetts and the Infrared Processing and Analysis Center, and funded by the National Aeronautics and Space Administration and the National Science Foundation. 2MASS data were obtained from the NASA/IPAC Infrared Science Archive, which is operated by the Jet Propulsion Laboratory, California Institute of Technology, under contract with the National Aeronautics and Space Administration. The authors wish to extend special thanks to those of Hawaiian ancestry on whose sacred mountain we are privileged to be guests.

Facilities: IRTF (SpeX); Magellan (LDSS-3)

REFERENCES

- Abell, G. O. 1959, *PASP*, 67, 258
 Allard, F. 1990, Ph.D. Thesis, Ruprecht-Karls University, Heidelberg
 Allard, F., & Hauschildt, P. H., 1995, *ApJ*, 445, 433
 Allard, F., Hauschildt, P. H., Alexander, D. R., & Starrfield, S. 1997, *ARA&A*, 35, 137
 Allard, F., Hauschildt, P. H., Alexander, D. R., Tamanai, A., & Schweitzer, A. 2001, *ApJ*, 556, 357
 Allard, F., Hauschildt, P. H., & Schwenke, D. 2000, *ApJ*, 540, 1005
 Allington-Smith, J., et al. 1994, *PASP*, 106, 983
 Bakos, G. Á., Sahu, K. C., & Németh, P. 2002, *ApJS*, 141, 187
 Baldwin, J. R., Frogel, J. A., & Persson, S. E. 1973, *ApJ*, 184, 427
 Baraffe, I., Chabrier, G., Allard, F., & Hauschildt, P. H. 1997, *A&A*, 327, 1054
 Bessell, M. S. 1982, *PASA*, 4, 417
 Bidelman, W. P., & Smethells, W. G. 1976, in *IAU Symp. 72, Abundance Effects in Classification* ed. B. Hauck, P. C. Keenan & W. W. Morgan (Boston: D. Reidel), p. 205
 Borysow, A., Jørgensen, U. G., & Zheng, C. 1997, *A&A*, 324, 185
 Burgasser, A. J. 2004 *ApJ*, 614, L73
 Burgasser, A. J., Geballe, T. R., Leggett, S. K., Kirkpatrick, J. D., & Golimowski, D. A. 2006 *ApJ*, in press
 Burgasser, A. J., Kirkpatrick, J. D., Burrows, A., Liebert, J., Reid, I. N., Gizis, J. E., McGovern, M. R., Prato, L., & McLean, I. S. 2003a, *ApJ*, 592, 1186
 Burgasser, A. J., Kirkpatrick, J. D., & Lépine, S. 2005 in *The 13th Cambridge Workshop on Cool Stars, Stellar Systems, and the Sun (ESA-SP-560)*, ed. F. Favata, G. A. J. Hussain & B. Battrock (Noordwijk: ESA), p. 237
 Burgasser, A. J., Kirkpatrick, J. D., McElwain, M. W., Cutri, R. M., Burgasser, A. J., & Skrutskie, M. F. 2003, *AJ*, 125, 850
 Burgasser, A. J., McElwain, M. W., Kirkpatrick, J. D., Cruz, K. L., Tinney, C. G., & Reid, I. N. 2004 *AJ*, 127, 2856
 Burrows, A., Dulick, M., Bauschlicher, C. W., Jr., Bernath, P. F., Ram, R. S., Sharp, C. M., & Milsom, J. 2005, *ApJ*, 624, 988
 Burrows, A., Hubbard, W. B., Lunine, J. I., & Liebert, J. 2001, *Rev. of Modern Physics*, 73, 719
 Cannon, R. D. 1984, in *Astronomy with Schmidt-Type Telescopes*, *Proc. IAU Coll. 78*, ed. M. Cappacioli (Dordrecht: Reidel), p. 25
 Carney, B., Latham, D., & Laird, J. B. 1988, *AJ*, 96, 560
 Corbally, C. J., Gray R. O., & Garrison, R. F. 1994, *The MK process at 50 years. A Powerful Tool for Astrophysical Insight* (San Francisco: Astronomical Society of the Pacific)
 Cottrell, P. L. 1978, *ApJ*, 223, 544
 Cushing, M. C., & Vacca, W. D. 2006, *AJ*, in press
 Cushing, M. C., Vacca, W. D., & Rayner, J. T. 2004, *PASP*, 116, 362
 Dawson, P. C., & De Robertis, M. M. 2000, *AJ*, 120, 1532
 Deacon, N. R., Hambly, N. C., & Cooke, J. A. 2005, *A&A*, 435, 363
 Dehnen, W., & Binney, J. J. 1998, *MNRAS*, 298, 387
 Epchtein, N., et al. 1997, *The Messenger*, 87, 27
 Gizis, J. E. 2002, *ApJ*, 575, 484
 Gizis, J. E. 1997, *AJ*, 113, 806 (G97)
 Gizis, J. E., Monet, D. G., Reid, I. N., Kirkpatrick, J. D., Liebert, J., & Williams, R. 2000, *AJ*, 120, 1085
 Gizis, J. E., & Reid, I. N. 1997, *PASP*, 109, 849
 —. 1999, *AJ*, 117, 508
 Golimowski, D. A., et al. 2004, *AJ*, 127, 3516
 Hambly, N. C., Davenhall, A. C., Irwin, M. J., & MacGillivray, H. T. 2001a, *MNRAS* 326, 1315
 Hambly, N. C., Irwin, M. J., & MacGillivray, H. T. 2001b, *MNRAS* 326, 1295
 Hambly, N. C., MacGillivray, H. T., Read, M. A., et al. 2001c, *MNRAS* 326, 1279
 Hambly, N. C., Henry, T. J., Subasavage, J. P., Brown, M. A., & Jao, W.-C. 2004, *AJ*, 128, 437
 Hamuy, M., Suntzeff, N. B., Heathcote, S. R., Walker, A. R., Gigoux, P., & Phillips, M. M. 1994, *PASP*, 106, 566
 Hartley, M., & Dawe, J. A. 1981, *PASA*, 4, 251
 Hauschildt, P. H., Allard, F., & Baron, E. 1999, *ApJ*, 512, 377
 Hauschildt, P. H., Baron, E., & Allard, F. 1997, *ApJ*, 483, 390
 Hawley, S. L., Gizis, J. E., & Reid, I. N. 1996, *AJ*, 112, 2799
 Hawley, S. L. et al. 2002, *AJ*, 123, 3409
 Hertzprung, R. J. 1905, *Zeit. Phot.*, 3, 429
 Jones, H. R. A., Longmore, A. J., Jameson, R. F., & Mountain, C. M. 1994, *MNRAS*, 267, 413
 Keenan, P. C., & McNeil, R. C. 1976, *An Atlas of Spectra of the Cooler Stars: Types G, K, M, S and C* (Columbus: Ohio State Univ. Press)
 Kerr, F. J., & Lynden-Bell, D. 1986, *MNRAS*, 221, 1023
 Kirkpatrick, J. D., Henry, T. J., & Irwin, M. J. 1997, *AJ*, 113, 1421
 Kirkpatrick, J. D., Henry, T. J., & McCarthy, D. W., Jr. 1991, *ApJS*, 77, 417
 Kirkpatrick, J. D., Kelly, D. M., Rieke, G. H., Liebert, J., Allard, F., & Wehrse, R. 1993, *ApJ*, 402, 643
 Kirkpatrick, J. D., et al. 1999, *ApJ*, 519, 802
 Kuiper, G. P. 1939, *ApJ*, 89, 549
 Kurucz, R. L. 1988, *Trans. IAU, XXB*, ed. M. McNally, (Dordrecht: Kluwer), p. 168-172
 Kurucz, R. L., & Bell, B. 1995, *Atomic Line Data*, Kurucz CD-ROM No. 23. (Cambridge: Smithsonian Astrophysical Observatory)
 Kurucz, R. L., & Peytremann, E. 1975, *SAO Special Report*, 362
 Leggett, S. K., Allard, F., Berriman, G., Dahn, C. C., & Hauschildt, P. H. 1996, *ApJS*, 104, 117

- Leggett, S. K., Allard, F., Dahn, C., Hauschildt, P. H., Kerr, T. H., & Rayner, J. 2000, *ApJ*, 535, 965
- Leggett, S. K., Allard, F., Geballe, T., Hauschildt, P. H., & Schweitzer, A. 2001, *ApJ*, 548, 908
- Leggett, S. K., Allard, F., & Hauschildt, P. H. 1998, *ApJ*, 509, 836
- Leonard, P. J. T., & Tremaine, S. 1990, *ApJ*, 353, 486
- Lépine, S., Rich, R. M., & Shara, M. M. 2003a, *AJ*, 125, 1598 (LRS03)
- Lépine, S., Rich, R. M., & Shara, M. M. 2003b, *ApJ*, 591, L49
- Lépine, S., & Shara, M. M. 2005, *AJ*, 129, 1483
- Lépine, S., Shara, M. M., & Rich, R. M. 2002, *AJ*, 124, 1190
- Lépine, S., Shara, M. M., & Rich, R. M. 2003, *ApJ*, 585, L69
- Lépine, S., Shara, M. M., & Rich, R. M. 2004, *ApJ*, 602, L125
- Liebert, J., & Probst, R. G. 1987, *ARA&A*, 25, 473
- Linsky, J. L. 1969, *ApJ*, 156, 989
- Lodders, K. 1999, *ApJ*, 519, 793
- Lodders, K. 2002, *ApJ*, 577, 974
- Lodieu, N., Scholz, R.-D., McCaughrean, M. J., Ibata, R., Irwin, M., & Zinnecker, H. 2005, *A&A*, 440, 1061
- Luyten, W. J. 1922, *Lick Obs. Bull.*, 10, 135
- Luyten, W. J. 1979a, *LHS Catalogue: A Catalogue of Stars with Proper Motions Exceeding 0^o.5 Annually* (Minneapolis: Univ. Minn. Press)
- . 1979b, *New Luyten Catalogue of Stars with Proper Motions Larger than Two Tenths of an Arcsecond (NLTT)* (Minneapolis: Univ. Minn. Press)
- Monet, D. G., Dahn, C. C., Vrba, F. J., Harris, H. C., Pier, J. R., Luginbuhl, C. B., & Ables, H. D. 1992, *AJ*, 103, 638
- Monet, D. G., et al. 2003, *AJ*, 125, 984 (USNO-B1.0 Catalog)
- Morgan, W. W., & Keenan, P. C. 1973, *ARA&A*, 11, 29
- Morgan, W. W., Keenan, P. C., & Kellman, E. 1943, *An Atlas of Stellar Spectra, with an Outline of Spectral Classification* (Chicago: Univ. Chicago Press)
- Morgan, W. W., Sharpless, S., & Osterbrock, D. 1952, *AJ*, 57, 3
- Morgan, D. H., Tritton, S. B., Savage, A., Hartley, M., & Cannon, R. D. 1992, in *Digitised Optical Sky Surveys*, ed. H. T. MacGillivray & E. B. Thomson (Dordrecht: Boston), p. 11
- Mould, J. R., & Hyland, A. R. 1976, *ApJ*, 208, 399
- Pokorny, R. S., Jones, H. R. A., & Hambly, N. C. 2003, *A&A*, 397, 575
- Pokorny, R. S., Jones, H. R. A., Hambly, N. C., & Pinfield, D. J. 2004, *A&A*, 421, 763
- Rayner, J. T., Toomey, D. W., Onaka, P. M., Denault, A. J., Stahlberger, W. E., Vacca, W. D., Cushing, M. C., & Wang, S. 2003, *PASP*, 155, 362
- Reid, I. N., & Hawley, S. L. 2000, *New Light on Dark Stars* (Chichester: Praxis)
- Reid, I. N., & Gizis, J. E. 2005, *PASP*, 117, 676
- Reid, I. N., Hawley, S. L., & Gizis, J. E. 1995, *AJ*, 110, 1838
- Reid, I. N., Kirkpatrick, J. D., Liebert, J., Gizis, J. E., Dahn, C. C., & Monet, D. G. 2002, *AJ*, 124, 519
- Reiners, A., & Basri, G. 2006, *AJ*, in press
- Reylé, C., & Robin, A. C. 2004, *A&A*, 421, 643
- Reylé, C., Robin, A. C., Scholz, R.-D., & Irwin, M. 2002, *A&A*, 390, 491
- Rojo, P., & Ruiz, M. T. 2003, *AJ*, 126, 353
- Ruiz, M. T., Wischnjewsky, M., Rojo, P. M., & Gonzalez, L. E. 2001, *ApJS*, 133, 119
- Salim, S., & Gould, A. 2002, *ApJ*, 575, L83
- Salim, S., & Gould, A. 2003, *ApJ*, 582, 1011
- Saumon, D., Bergeron, P., Lunine, J. I., Hubbard, W. B., & Burrows, A. 1994, *ApJ*, 424, 333
- Scholz, R.-D., Irwin, M., Ibata, R., Jahreiß, H., & Malkov, O. Yu. 2000, *A&A*, 353, 958
- Scholz, R.-D., Lehmann, I., Matute, I., & Zinnecker, H. 2004, *A&A*, 425, 519
- Scholz, R.-D., Lodieu, J., & McCaughrean, M. 2004, *A&A*, 428, L25
- Schweitzer, A., Shultz, R.-D., Stauffer, J., Irwin, M., & McCaughrean, M. J. 1999, *A&A*, 350, L62
- Skrutskie, M. F., et al. 2006, *AJ*, 131, 1163
- Subasavage, J. P., Henry, T. J., Hambly, N. C., Brown, M. A., & Jao, W.-C. 2005a, *AJ*, 129, 413
- Subasavage, J. P., Henry, T. J., Hambly, N. C., Brown, M. A., Jao, W.-C., & Finch, C. T. 2005b, *AJ*, 130, 1658
- Vacca, W. D., Cushing, M. C., & Rayner, J. T. 2003, *PASP*, 155, 389
- Warner, B. 1968, *MNRAS*, 140, 53
- West, A. A., et al. 2004, *AJ*, 128, 426
- West, R. M. 1984, in *Astronomy with Schmidt-Type Telescopes*, *Proc. IAU Coll. 78*, ed. M. Cappaccioli (Dordrecht: Reidel), p. 13
- West, R. M., & Schuster, H.-E. 1982, *A&AS*, 49, 577
- Wiese, W. L., Smith, M. W., & Glennon, B. M. 1966, *Atomic Transition Probabilities, Vol. 1*. (Washington, D. C.: GPO)
- York, D. G., et al. 2000, *AJ*, 120, 1579

FIG. 1.— H_J versus $(R_{ESO} - J)$ diagram for the LEHPM catalog (Pokorny et al. 2004). Note the three clusters of sources corresponding to (from center to lower left) main sequence dwarfs, halo subdwarfs and white dwarfs. Our selection criteria for ultracool dwarf and subdwarf candidates are indicated by dashed lines. Previously classified sources within this region are noted by open circles; LEHPM 2-59 is indicated by an open square. [THIS FIGURE IS INCLUDED IN JPEG FORMAT]

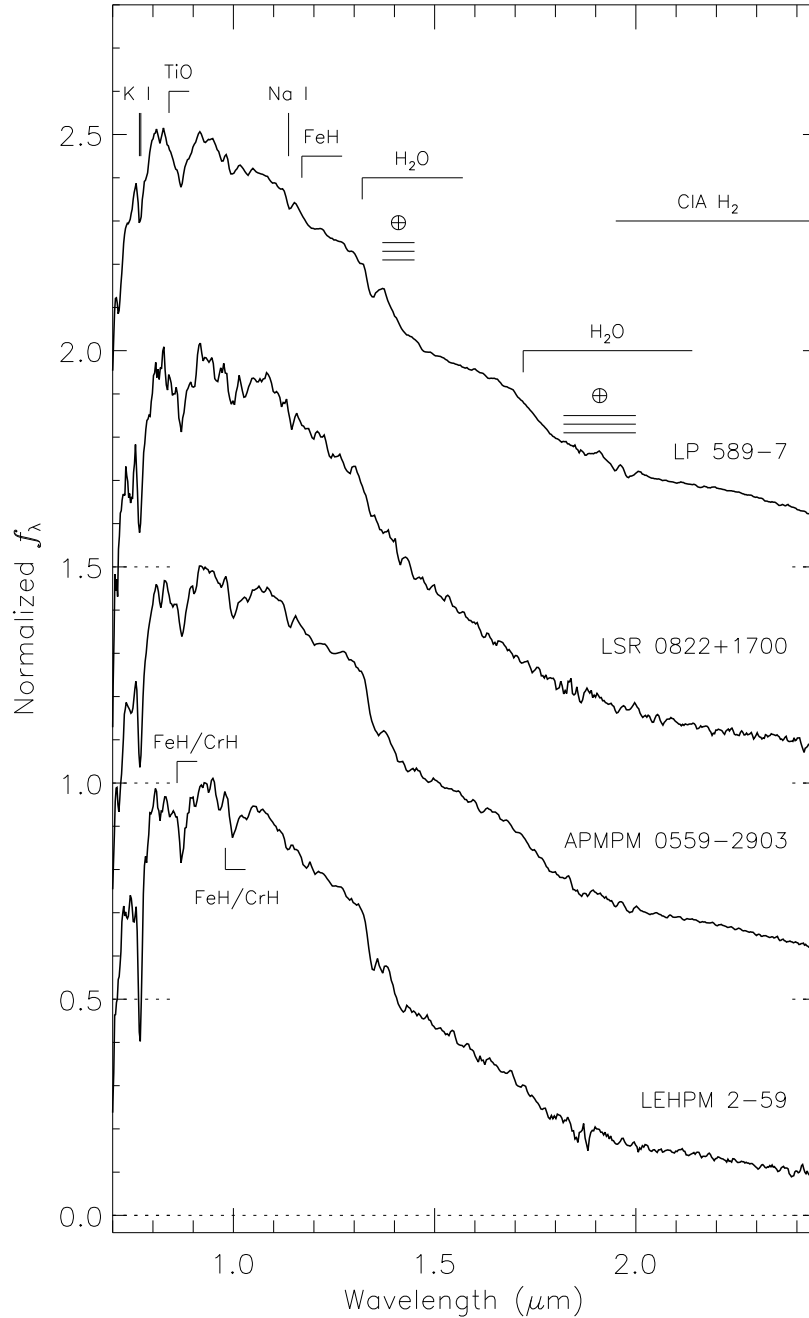


FIG. 2.— SpeX prism spectra of the esdMs LP 589-7 (esdM5), LSR 0822+1700 (esdM6.5), APMPM 0559-2903 (esdM7) and LEHPM 2-59 (esdM8). Spectra are normalized at their flux peaks and offset by constants (dotted lines). Prominent features in the NIR spectra of cool esdMs discernible at the resolution of these prism data ($\lambda/\Delta\lambda \approx 150$) are labeled. Regions of high telluric opacity are indicated by \oplus symbols.

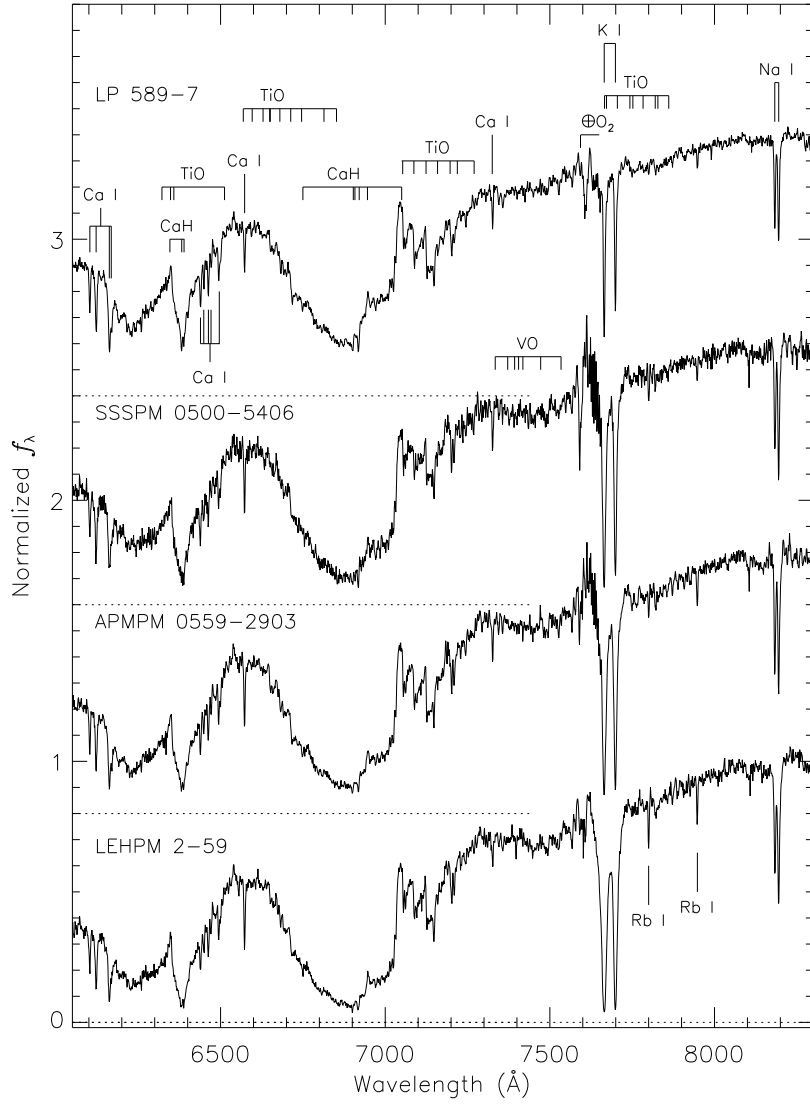


FIG. 3.— Optical spectra of the late esdMs LP 589-7 (esdM5), SSSPM 0500-5406 (esdM6.5), APMPM 0559-2903 (esdM7) and LEHPM 2-59 (esdM8) from top to bottom. All data are shifted to their rest frame velocities, normalized at 8100 Å and offset by a constant (dotted lines). Identified molecular features are from Kirkpatrick, Henry, & McCarthy (1991); atomic features are from Kurucz & Bell (1995, see Table 3). Residual noise from the telluric O₂ A-band is indicated by ⊕ symbols.

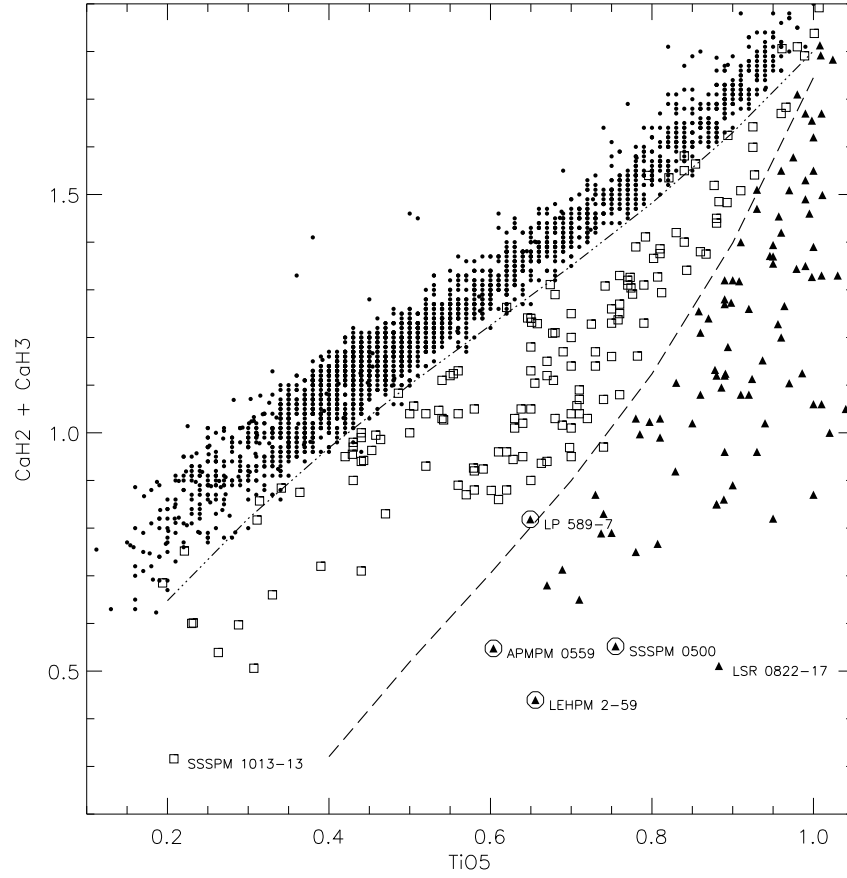


FIG. 4.— Spectral indices $\text{CaH2} + \text{CaH3}$ versus TiO5 for dwarfs (points), subdwarfs (open squares) and extreme subdwarfs (filled triangles) from Hawley, Gizis, & Reid (1996); G97; Gizis & Reid (1997); Reid et al. (2002); LRS03; Lépine, Shara, & Rich (2004); and Scholz et al. (2004a). Data from this paper are encircled and labeled, while values for the esdM6.5 LSR 0822+1700 and the sdM9.5 SSSPM 1013-1356 from Lépine, Shara, & Rich (2004) and Scholz et al. (2004a), respectively, are also labeled. Dashed lines delineate boundaries between dwarfs, sdMs and esdMs as defined by Eqns. 1 and 2.

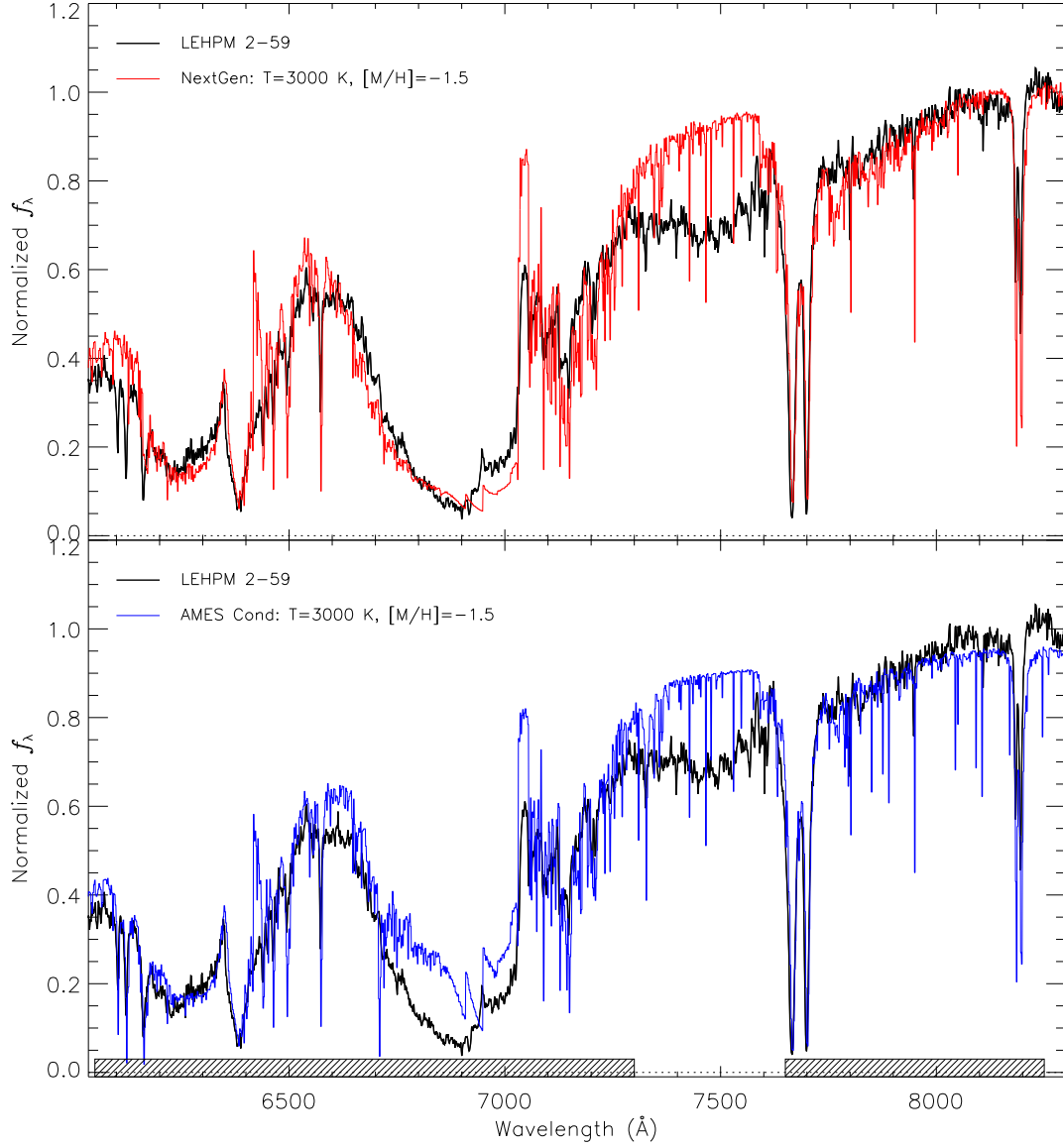


FIG. 5.— Comparison of best fit NextGen (top) and AMES Cond (bottom) $\log g = 5.0 \text{ cm s}^{-1}$ models to the observed red optical spectrum of LEHPM 2-59 (black). LEHPM 2-59 spectra are normalized at 8100 \AA ; model spectra are scaled to their best fit normalization. The wavelength ranges for which spectral data and models were compared are indicated by the hatched areas.

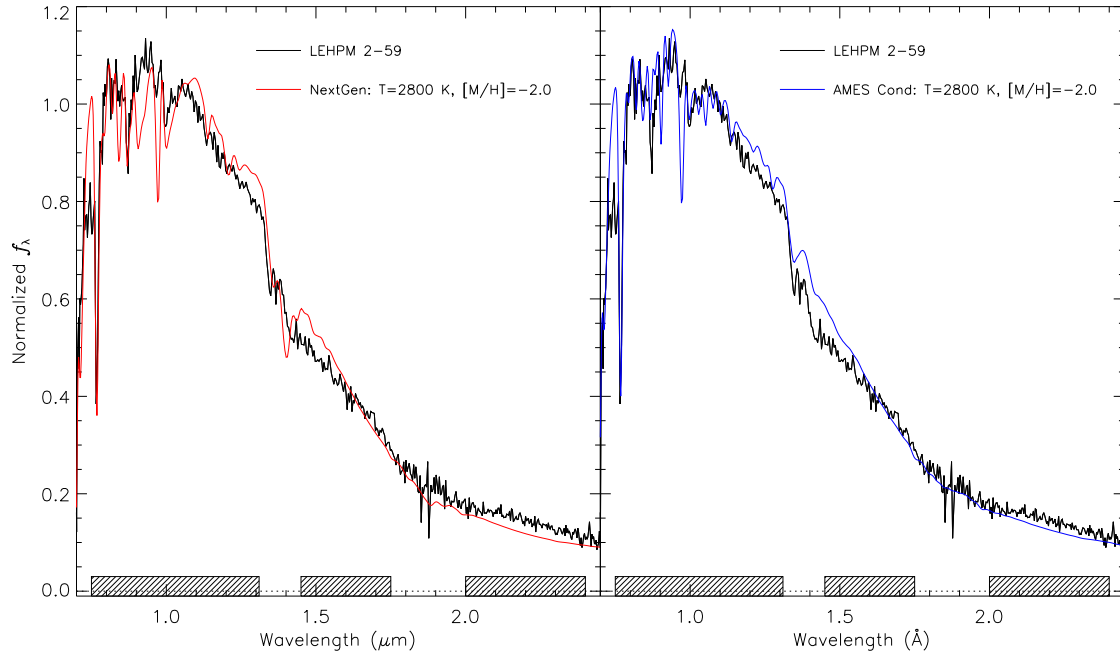


FIG. 6.— Same as Fig. 5 for near infrared spectral fits to LEHPM 2-59. Spectra are normalized at $1.05\ \mu\text{m}$.

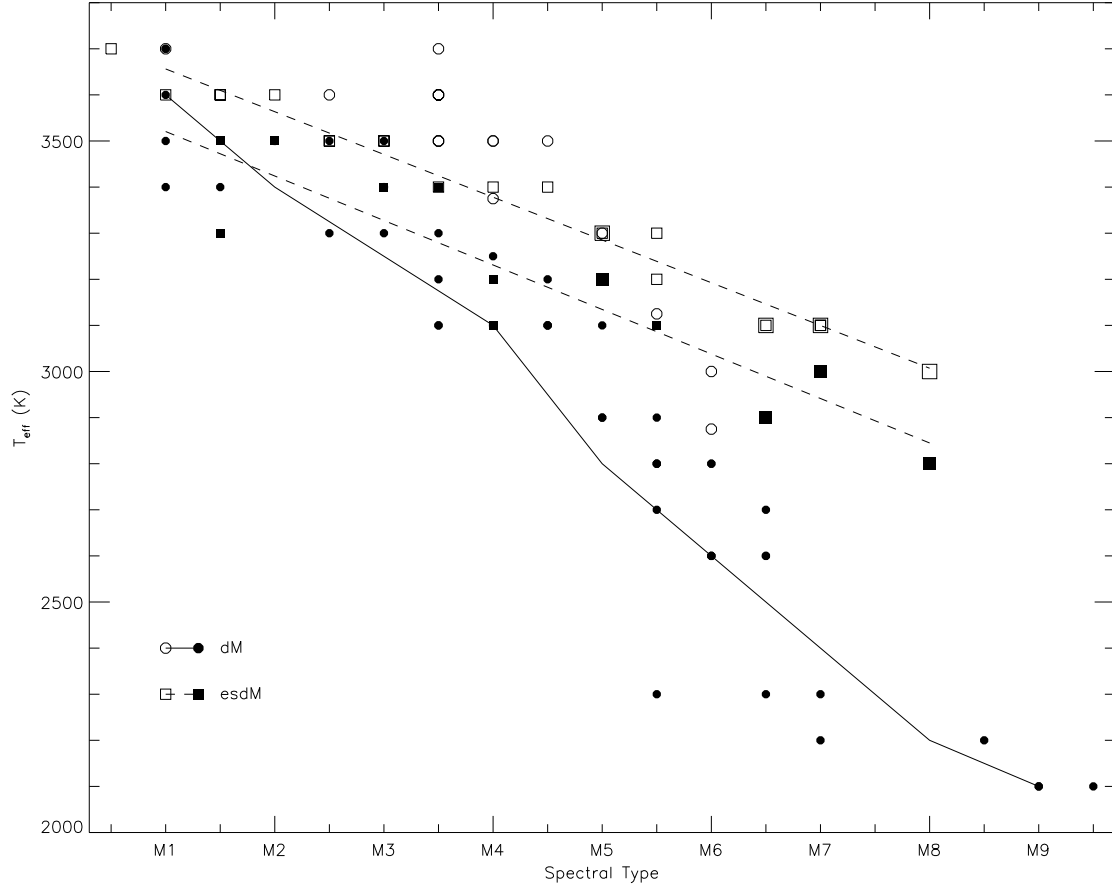


FIG. 7.— T_{eff} s for field M dwarfs (circles) and esdMs (squares) based on spectral model fits. Data are from Kirkpatrick et al. (1993, SpT \leq M6); Leggett et al. (1996, 2000, 2001); Gizis (1997, SpT \leq M6); Schweitzer et al. (1999); Lépine, Shara, & Rich (2004); and this paper (oversize symbols). T_{eff} s derived from fits to optical data are indicated by open symbols, those from near infrared data by solid symbols. The solid line delineates the M dwarf T_{eff} scale from Reid & Hawley (2000); the dashed lines delineate linear fits for esdM T_{eff} s based on optical (top) and near infrared (bottom) data (Eqns. 10 and 11).

TABLE 1
SPEX OBSERVING LOG

Source	α^a	δ^a	J^b	UT Date	t_{int} (s)	Airmass	Flux Cal.	SpT	Ref. ^c
LP 589-7	01 ^h 57 ^m 27 ^s .92	+01° 16 ^m 43 ^s .3	14.50±0.03	2004 Sep 5	1080	1.13	HD 13936	A0 V	1
LEHPM 2-59	04 ^h 52 ^m 09 ^s .94	-22° 45 ^m 08 ^s .4	15.52±0.05	2004 Sep 9	720	1.43	HD 32855	A0 V	2
APMPM 0559-2903	05 ^h 58 ^m 58 ^s .91	-29° 03 ^m 26 ^s .7	14.89±0.04	2005 Dec 31	1440	1.53	HD 41473	A0 V	3
LSR 0822-1700	08 ^h 22 ^m 33 ^s .69	-17° 00 ^m 19 ^s .9	15.87±0.08	2004 Mar 10	1080	1.01	HD 58383	A0 V	4

REFERENCES. — (1) Gizis & Reid (1999); (2) Pokorny et al. (2004); (3) Schweitzer et al. (1999); (4) Lépine, Shara, & Rich (2004)

^aJ2000 Coordinates from 2MASS.

^b J magnitudes from 2MASS.

^cDiscovery reference for esdM source.

TABLE 2
LDSS-3 OBSERVING LOG

Source	α^a	δ^a	R^b	UT Date	t_{int} (s)	Airmass	Tell. Cal.	SpT	Ref. ^c
LP 589-7	01 ^h 57 ^m 27 ^s .92	+01° 16 ^m 43 ^s .3	17.39	2005 Dec 4	2100	1.16	HD 603	G2 V	1
LEHPM 2-59	04 ^h 52 ^m 09 ^s .94	-22° 45 ^m 08 ^s .4	18.72	2005 Dec 4	1800	1.04	HD 31527	G2 V	2
SSSPM 0500-5406	05 ^h 00 ^m 15 ^s .77	-54° 06 ^m 27 ^s .3	17.42	2005 Dec 4	600	1.50	HD 33967	G2/3 V	3
APMPM 0559-2903	05 ^h 58 ^m 58 ^s .91	-29° 03 ^m 26 ^s .7	18.08	2005 Dec 4	1200	1.06	HD 33967	G2/3 V	4

REFERENCES. — (1) Gizis & Reid (1999); (2) Pokorny et al. (2004); (3) Lodieu et al. (2005); (4) Schweitzer et al. (1999).

^aJ2000 Coordinates from 2MASS.

^bPhotographic R magnitudes from the SuperCosmos Sky Survey.

^cDiscovery reference for esdM source.

TABLE 3
ATOMIC LINES IDENTIFIED IN ESDM OPTICAL SPECTRA
OVER $\lambda\lambda$ 6100–8300 Å

Wavelength (Å)	Element	E_{lower} (eV)	E_{upper} (eV)	Ref.
6102.723	Ca I	1.879467	3.910663	1
6122.217	Ca I	1.885935	3.910663	1
6162.173	Ca I	1.899063	3.910663	1
6166.439 ^a	Ca I	2.521433	4.531641	1
6169.042 ^a	Ca I	2.523157	4.532517	1
6169.563 ^a	Ca I	2.525852	4.535043	1
6439.075	Ca I	2.525852	4.450947	1
6449.808	Ca I	2.521433	4.443325	1
6462.567	Ca I	2.523157	4.441254	1
6471.662	Ca I	2.525852	4.441254	1
6493.781 ^a	Ca I	2.521433	4.430310	1
6499.650 ^a	Ca I	2.523157	4.430310	1
6572.779	Ca I	0.000000	1.885935	1
6717.681	Ca I	2.709192	4.554447	1
7148.150	Ca I	2.709192	4.443325	2
7202.200	Ca I	2.709192	4.430310	2
7326.145	Ca I	2.932710	4.624710	2
7664.911	K I	0.000000	1.617220	1
7698.974	K I	0.000000	1.610064	1
7800.259	Rb I	0.000000	1.589158	3
7947.597	Rb I	0.000000	1.559697	3
8183.255	Na I	2.102439	3.617221	4
8194.790 ^a	Na I	2.104571	3.617221	4
8194.824 ^a	Na I	2.104571	3.617215	4

REFERENCES. — (1) Wiese, Smith, & Glennon (1966); (2) Kurucz (1988); (3) Warner (1968); (4) Kurucz & Peytremann (1975).

^aBlend.

TABLE 4
ALKALI ATOMIC LINE EQUIVALENT WIDTHS (Å).

Source	Ca I (6573 Å)	Ca I (7326 Å)	K I (7665/7699 Å)	Rb I (7800 Å)	Rb I (7948 Å)	Na I (8183/8195 Å)	V_{rad} (km s ⁻¹)
LP 589-7	1.17±0.06	0.76±0.08	9±2	<0.10	0.28±0.03	4.54±0.14	-82±9
SSSPM 0500-5406	2.03±0.15	0.99±0.16	26±2	<0.15	0.5±0.2	6.5±0.4	216±9
APMPM 0559-2903	2.0±0.2	1.1±0.2	27.7±1.9	0.34±0.10	0.62±0.11	6.74±0.14	181±5
LEHPM 2-59	2.17±0.13	0.93±0.12	39.7±1.2	0.60±0.07	0.68±0.05	7.2±0.3	79±9

TABLE 5
SPECTRAL RATIOS AND CLASSIFICATION.

Source	CaH1	CaH2 ^a	CaH3 ^a	TiO5	Color-M ^a	SpT
LP 589-7	0.472	0.325 (4.8)	0.493 (4.9)	0.649	1.49 (4.7)	sd/esdM5
SSSPM 0500-5406	0.310	0.220 (6.5)	0.331 (7.0)	0.755	1.64 (6.8)	esdM6.5
APMPM 0559-2903	0.342	0.217 (6.6)	0.331 (7.0)	0.604	1.67 (7.1)	esdM7
LEHPM 2-59	0.267	0.175 (7.3)	0.265 (7.9)	0.656	1.79 (8.7)	esdM8

^aNumerical esdM subtype in parentheses based on Eqns. 1-3.

TABLE 6
SPECTRAL MODEL FITS.^a

Source	SpT	NextGen				AMES Cond			
		5.0 ^b		5.5		5.0		5.5	
		T_{eff} (K)	[M/H] (dex)	T_{eff} (K)	[M/H] (dex)	T_{eff} (K)	[M/H] (dex)	T_{eff} (K)	[M/H] (dex)
Optical									
LP 589-7	sd/esdM5	3300	-1.0	3300	-1.0	3200	-1.0	3300	-1.0
SSSPM 0500-5406	esdM6.5	3100	-1.5	3200	-1.5	3000	-1.5	3200	-1.0
APMPM 0559-2903	esdM7	3100	-1.5	3200	-1.0	3000	-1.5	3100	-1.0
LEHPM 2-59	esdM8	3000	-1.5	3100	-1.5	3000	-1.5	3100	-1.0
Near Infrared									
LP 589-7	sd/esdM5	3200	-2.0	3300	-1.5	3200	-2.0	3200	-1.5
LSR 0822+1700	esdM6.5	2900	-2.0	3000	-2.0	2900	-2.0	3000	-2.0
APMPM 0559-2903	esdM7	3000	-2.0	3100	-1.5	3000	-1.5	3000	-1.5
LEHPM 2-59	esdM8	2800	-2.0	3000	-2.0	2800	-2.0	3000	-2.0

^aValues in bold denote overall best fit models.

^bLogarithm of surface gravity in cm s⁻².

TABLE 7
 PROPERTIES OF LEHPM 2-59.

Parameter	Value	Ref.
α^a	04 ^h 52 ^m 09 ^{''} 94	1
δ^a	-22° 45 ^m 08 ^{''} 4	1
SpT	esdM8	2,3,4
R_{ESO}^b	18.72	5,6
R_{USNO}^b	18.82	7
I_{SSS}^b	16.86	5,6
I_{USNO}^b	17.24	7
I_{DENIS}	16.74±0.09	8
J	15.52±0.05	1
H	15.25±0.08	1
K_s	14.76±0.11	1
μ	0 ^{''} 746±0 ^{''} 016 yr ⁻¹	6
θ	174° 7±1° 2	6
d_{est}	66±15 pc	2,4
V_{rad}	79±8 km s ⁻¹	2
$[U, V, W]^c$	[135,-180,-80] km s ⁻¹	2
T_{eff}	2800-3000 K	2
$[M/H]$	-1.5 to -2.0	2

REFERENCES. — (1) 2MASS; (2) This paper; (3) Gizis (1997); (4) Lépine, Rich, & Shara (2003a); (5) SSS (Hambly et al. 2001a,b,c); (6) Pokorny et al. (2004); (7) USNO-B1.0 (Monet et al. 2003); (8) DENIS (Epchtein et al. 1997).

^a2MASS coordinates, equinox J2000 and epoch 1998 Nov 29 (UT).

^bPhotographic R (IIIaF) and I_N (IV-N) magnitudes.

^cAssuming a distance of 66 pc.

This figure "f1.jpg" is available in "jpg" format from:

<http://arxiv.org/ps/astro-ph/0603382v1>